Nanoscale

PAPER

Cite this: *Nanoscale*, 2016, **8**, 15348

Towards ALD thin film stabilized single-atom Pd_1 catalysts†

Mar Piernavieja-Hermida,[a] Zheng Lu,[a] Anderson White,[a] Ke-Bin Low,[b] Tianpin Wu,[c] Jeffrey W. Elam,[d] Zili Wu[e] and Yu Lei*[a]

Received 31st May 2016,
Accepted 22nd July 2016

DOI: 10.1039/c6nr04403d

www.rsc.org/nanoscale

Supported precious metal single-atom catalysts have shown interesting activity and selectivity in recent studies. However, agglomeration of these highly mobile mononuclear surface species can eliminate their unique catalytic properties. Here we study a strategy for synthesizing thin film stabilized single-atom Pd_1 catalysts using atomic layer deposition (ALD). The thermal stability of the Pd_1 catalysts is significantly enhanced by creating a nanocavity thin film structure. *In situ* infrared spectroscopy and Pd K-edge X-ray absorption spectroscopy (XAS) revealed that the Pd_1 was anchored on the surface through chlorine sites. The thin film stabilized Pd_1 catalysts were thermally stable under both oxidation and reduction conditions. The catalytic performance in the methanol decomposition reaction is found to depend on the thickness of protecting layers. While Pd_1 catalysts showed promising activity at low temperature in a methanol decomposition reaction, 14 cycle TiO_2 protected Pd_1 was less active at high temperature. Pd L_3 edge XAS indicated that the low reactivity compared with Pd nanoparticles is due to the strong adsorption of carbon monoxide even at 250 °C. These results clearly show that the ALD nanocavities provide a basis for future design of single-atom catalysts that are highly efficient and stable.

Introduction

Nanomaterials are known to possess dramatically different electronic, chemical, and physical properties compared to their bulk counterparts.[1–6] For instance, when the dimensions of supported precious metals approach the nanometer and subnanometer scale, unique catalytic properties emerge related to under-coordinated surface atoms, electronic structures, and diffusion barriers of surface species. In ultra-high vacuum (UHV) experiments using well-defined single crystals, Heiz and Schneider were the first to observe size-dependent catalytic activity in an atom-by-atom fashion for CO oxidation by gold clusters[7] and the cyclotrimerization of acetylene by palladium clusters.[8] Since then, significant research has been performed to explore size-dependent catalysis with atomic precision using the so-called size-selected cluster deposition technique.[9–13] More recently, in a combined scanning tunneling microscopy (STM), DFT and temperature-programmed desorption (TPD) study, Flytzani-Stephanopoulos and Sykes found that isolated Pd_1 atoms alloyed with the Cu(111) surface showed highly selective hydrogenation of styrene and acetylene.[14] The improved selectivity was attributed to low-barrier hydrogen dissociation at Pd atom sites and weak binding of the products to Cu.

The preparation of a site-isolated single atom supported on high surface area oxide catalysts has recently been realized *via* wet chemistry. The single atom catalysts have shown unexpectedly high activity and selectivity to valuable products under realistic catalytic reaction conditions. Single-atom Pt_1 supported by FeO_x nanocrystallite substrates showed extremely high atom efficiency for preferential oxidation of CO in H_2.[15] DFT calculations showed that the high activity and selectivity are correlated with the partially vacant 5d orbitals of positively charged, high-valent Pt atoms. Other successful examples at the lab scale include well-defined Pt_1,[16] Pd_1,[17] Rh_1,[18] Au_1,[19–21] and Ir_1.[22] In industrial scale production, titanium silicalite (TS-1) is a commercial catalyst for propylene epoxidation with hydrogen peroxide.[23] The isolated Ti active sites of TS-1 provide a high selectivity towards propylene oxide, since propylene oxide molecules that adsorb on adjacent Ti sites lead to catalyst deactivation and the formation of unwanted byproducts.[24–27]

[a]*Department of Chemical and Materials Engineering, University of Alabama in Huntsville, Huntsville, Alabama 35899, USA. E-mail: yu.lei@uah.edu*
[b]*Research Resources Center, University of Illinois at Chicago, Chicago, Illinois 60607, USA*
[c]*X-ray Science Division, Argonne National Laboratory, Argonne, Illinois 60439, USA*
[d]*Energy Systems Division, Argonne National Laboratory, Argonne, Illinois 60439, USA*
[e]*Center for Nanophase Materials Sciences and Chemical Science Division, Oak Ridge National Laboratory, Oak Ridge, Tennessee 37831, USA*

†Electronic supplementary information (ESI) available: Extended experimental details and supplementary STEM images, XRD, QCM, BET, EXAFS. See DOI: 10.1039/c6nr04403d

Despite these successes, the thermal stability of precious metal single site catalysts under reaction conditions remains a significant challenge. The synthesis of a highly active single-atom catalyst with improved thermal stability attracts both fundamental and industrial interest.[28] In addition, obtaining uniform, thermally stable single atom catalysts under reaction conditions is a critical step towards precisely identifying catalyst active sites. Here we demonstrate an approach to improve the thermal stability of uniformly dispersed Pd_1 single atom catalysts using ultrathin metal oxide protective coatings prepared by atomic layer deposition (ALD).

Experimental

Catalyst synthesis

The Pd catalyst materials were synthesized using a commercial benchtop ALD reactor (Arradiance, Gemstar-6) equipped with an *in situ* quartz-crystal microbalance (QCM, Inficon). Ultrahigh purity nitrogen carrier gas (Airgas, 99.999%) was further purified using a Supelco gas purifier (Sigma-Aldrich) to trap hydrocarbon, moisture and oxygen-containing impurities before entering the reactor.

Spherical alumina powder (NanoDur, 99.5%, Alfa Aesar) was used as a substrate without further treatment. The substrate was uniformly spread onto a stainless steel sample tray with a stainless steel mesh top to contain the powder while still supplying access to the ALD precursor vapor. The loaded sample tray was placed into the center of the reactor and kept for at least 30 min at 200 °C in a 50 sccm flow at 0.5 Torr pressure to allow temperature stabilization.

The ALD timing sequences can be expressed as t_1–t_2–t_3–t_4, where t_1 and t_3 correspond to the exposure times of the two precursors, t_2 and t_4 are the nitrogen purge times between precursor exposures and all units are given in seconds. 500 mg of Al_2O_3 NanoDur was modified using 3 ALD cycles of TiO_2. The TiO_2 coating used alternating exposures to $TiCl_4$ (Sigma-Aldrich, 99.9%) and deionized water with a time sequence (80 s–160 s–80 s–160 s) at 150 °C. For the TiO_2 overcoat, 1, 7, and 14 cycles were used. The Pd ALD used exposures to Pd(II) hexafluoroacetylacetonate ($Pd(hfac)_2$, Sigma-Aldrich, 98%) at 100 °C with a time sequence (300 s–300 s) at 100 °C. The samples were denoted as $1cTiPd_1$, $7cTiPd_1$, and $14cTiPd_1$, respectively. For each sample, the mass was measured with an analytical balance before and after ALD to determine the Pd loading. The weight percent of palladium in Pd_1 catalysts was estimated to be 0.5 wt%.

Characterization

Quartz Crystal Microbalance (QCM) studies were performed for Pd ALD using a Maxtek BSH-150 bakeable sensor, AT-cut quartz sensor crystals (Colorado Crystal Corporation), and a Maxtek TM400 film thickness monitor. To monitor the Pd growth on Al_2O_3 and TiO_2 supports with QCM, a thick layer (3 nm) of Al_2O_3 or TiO_2 was first deposited on the QCM at the same temperature as used for Pd ALD. The Al_2O_3 layer was grown by sequential exposures of TMA and water for about 60 cycles; TiO_2 was grown by sequential exposure of TTIP and water for 100 cycles; and Pd was grown by sequential exposures of $Pd(hfac)_2$ and formalin. The QCM mass measurements were converted to Pd film thicknesses assuming a density of 12.0 g cm^{-3} for Pd.

Brunauer–Emmett–Teller (BET) surface areas of all palladium catalysts were measured *via* nitrogen adsorption at 77 K by using a Micromeritics Gemini 275 system. The surface composition of the as-prepared $TiPd_1$ catalysts was analyzed using an X-ray photoemission spectroscopy (XPS, Kratos AXIS-165) system using a monochromatic Al Kα (1486.6 eV) X-ray source operating at 15 kV and 10 mA.

Microscopy characterization was performed on an aberration-corrected scanning transmission electron microscope (STEM) equipped with a 200 keV Schottky cold-field emission gun, a high-angle annular dark field (HAADF) detector, and an annular bright field (ABF) detector.

Pd K-edge (23.564 keV) X-ray absorption spectroscopy (XAS) was performed at the 10-BM beamline at the Advanced Photon Source (APS) at Argonne National Laboratory. The amount of the sample in use was optimized to achieve an XAS step height of about 1. The XAS spectra were recorded in transmission mode. Standard procedures based on WINXAS 3.1 software were used to fit the data in the extended X-ray absorption fine structure (EXAFS) regime.

Pd L_3-edge (3.173 keV) XAS was carried out at the 9-BM beamline at the APS. The sample was measured in the fluorescence mode. The Pd catalysts were pressed as a pellet and installed in a stainless steel sample holder housed in an aluminum environmental chamber. The temperature of the sample holder was controlled using K-type thermocouples and a ceramic heating plate. The catalyst of interest was first reduced in 3.5% hydrogen/helium at 250 °C for 30 minutes. Then ultrahigh purity helium was used to purge the chamber at 250 °C to remove the hydrogen. The resultant catalyst was fully reduced Pd without adsorbate. X-ray absorption near edge structure (XANES) spectra were recorded for the clean Pd surface. The system was then purged with 10 sccm flow of 1% CO to generate CO adsorbed Pd. XANES were then recorded under the steady state flow of CO. Multiple XANES spectra were recorded and averaged to enhance signal to noise.

Diffuse Reflectance Infrared Fourier Transform Spectroscopy (DRIFTS) measurements on CO adsorption were performed using a Thermo Nicolet Nexus 670 spectrometer, with a MCT/A detector with a spectral resolution of 4 cm^{-1}, in diffuse reflectance mode while the exiting stream was analyzed by QMS. A Pike Technologies HC-900 DRIFTS cell with a nominal cell volume of 6 cm^3 was used. Before each of the following IR experiments, the palladium sample was pretreated in the DRIFTS cell in flowing 4% H_2/He (25 mL min^{-1}) at 250 °C for 30 minutes and then cooled to room temperature.

In CO adsorption experiments, the pretreated sample was purged with helium at room temperature before switching to 2%CO/2%Ar/He (25 mL min^{-1}) flow for 30 min. The sample was then purged with helium at rt for another 30 min. IR

spectra and QMS profiles were recorded continuously during these processes. All reported IR spectra are difference spectra referenced to a background spectrum collected after pretreatment but prior to CO adsorption.

The *in situ* FT-IR measurements under the practical ALD conditions for TiO_2 overcoating were conducted in a specially design ALD reactor described previously.[29] The FT-IR data were collected using a Thermo Scientific Nicolet 6700 FT-IR spectrometer. ZrO_2 powder was used as the substrate and pressed into a metal grid. Pd and TiO_2 ALD were subsequently performed. The ALD recipes are identical to those described in the catalyst synthesis section. FT-IR spectra were recorded after each chemical exposure.

Catalytic performance

For each test, 30 mg of Pd catalysts were used on a plug-flow, temperature-controlled microreactor system (Altamira AMI 300). The sample, loaded into a U-shaped quartz tube (4 mm i.d.) and supported by quartz wool, was pretreated in flowing 4% H_2/He (25 mL min^{-1}) at 250 °C for 30 minutes and cooled down to room temperature (RT) in a He atmosphere. In the case of methanol decomposition, He was bubbled through methanol at 25 cm^3 min^{-1}. All gases were provided by Air Liquide with the ultrahigh purity (UHP, 99.999%) helium as balance gas.

A downstream quadrupole mass spectrometer (QMS) was utilized in order to obtain the catalytic activity of the Pd catalysts by using a methanol decomposition reaction. A calibration experiment was performed where methanol was kept at temperatures 5 °C, 10 °C, 15 °C and 20 °C (using a water bath) until the QMS was stabilized at each temperature, and the respective intensities of methanol (monitored at *m*/*z* 31) were recorded. A linear fit of the respective intensities *versus* the methanol concentration at the indicated temperatures, obtained from the vapor pressures, was plotted. The intensity and slope were then utilized to calculate the respective methanol concentrations for the different catalyst reactions. During the decomposition reaction, methanol was kept at 20 °C, therefore the methanol conversion was calculated using different concentrations of methanol during the reaction and the concentration at 20 °C.

In order to quantify the amount of CO adsorbed on the Pd surface, CO pulse chemisorption was carried out on a plug-flow microreactor system (Altamira AMI 300) and a downstream quadrupole mass spectrometer (QMS) (OmniStar GSD-301 O_2, Pfeiffer Vacuum). Approximately 35 mg of the sample was loaded in a U-shaped microreactor and reduced in 4% H_2/He (25 mL min^{-1}) at 250 °C for 30 minutes. The sample was cooled down to room temperature in He (25 mL min^{-1}). After being stabilized at room temperature, 2%CO/2% Ar/He was pulsed multiple times onto the sample in a He flow (25 mL min^{-1}), and a mass spectrum was collected until there was no change in the CO peak intensity monitored by QMS. One pulse of CO was brought to the sample *via* a 6-way valve, with a volume of 0.5 cm^3. The CO peak intensity was calibrated by pulsing 2%CO/2%Ar/He through the reactor bypass.

Results and discussion

ALD is a deposition technique that enables conformal coatings of both nanoparticles and thin films on high-aspect-ratio substrates.[30,31] It represents a promising, alternative method to synthesize and tailor nanostructured catalysts.[32–35] The strategy used to synthesize stable Pd_1 single atom catalysts is described in Scheme 1. Palladium hexafluoroacetylacetonate ($Pd(hfac)_2$) is used as the ALD metal precursor for preparing the Pd catalyst (see Fig. S1†). After chemisorbing $Pd(hfac)_2$ onto the substrate surface (1), the remaining hfac ligands prevent growth on the Pd during the subsequent metal oxide ALD. ALD TiO_2 is deposited using alternating exposures to titanium tetrachloride ($TiCl_4$) and deionized water, but the TiO_2 grows selectively on the substrate and not on the chemisorbed $Pd(hfac)_2$ (2). As a consequence, the bulky structure of the –hfac ligands of diameter of *ca.* 5.2 Å templates the formation of a nanocavity of similar dimension around the Pd. Finally, the –hfac ligands are removed using formalin (HCHO) to generate TiO_2 nanocavity protected Pd_1 sites (3). 1-Cycle, 7-cycle and 14-cycle TiO_2 thin film stabilized Pd_1 were prepared using this strategy, denoted as 1TiPd, 7TiPd and 14TiPd, respectively. The equivalent thicknesses of these thin films are 0.7 Å, 4.7 Å, and 9.4 Å, for 1c, 7c and 14c TiO_2, respectively, determined using an *in situ* quartz crystal microbalance (QCM) (see Fig. S2†). In particular, the nanocavity generated using 7c TiO_2 has a similar height of the surface Pd(hfac) species, while the depth of 14c TiO_2 is about twice the height of Pd(hfac). An unprotected Pd sample (0TiPd) was also synthesized and used as a reference.

TiO_2 was selected as the material to form the nanocavity because of several reasons. First of all, TiO_2 ALD processes have been well-established in the literature and can be performed under mild conditions.[36,37] Secondly, these processes offer uniform coatings of TiO_2, which is critical to prepare well-defined nanocavities on high-aspect-ratio substrates for heterogeneous catalysts. Last but not least, Pd/TiO_2 typically shows a strong metal support interaction (SMSI) after reduction at high temperature (*e.g.*, above 473 K), which could potentially improve the thermal stability of Pd_1 atoms. All of the ALD TiO_2 stabilized Pd_1 catalysts were prepared on commercial spherical aluminum oxide nanoparticles (Al_2O_3, Alfa Aesar, NanoDur™, 99.5%). Brunauer–Emmett–Teller (BET) surface area measurements showed that the ALD TiO_2 stabilized Pd_1 treatment did not change the surface area of the substrate. The bare Al_2O_3 substrate and all the ALD catalysts have a surface area of ~33 m^2 g^{-1} (see Table S1 and Fig. S3†). X-ray

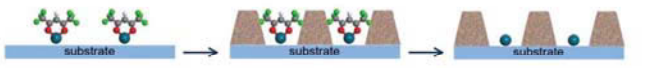

Scheme 1 Schematics of thermally stable Pd_1 catalysts synthesized using ALD. (1) Depositing Pd(hfac) on spherical Al_2O_3 substrate, (2) creating nanocavity structure using TiO_2 ALD, and (3) removing –hfac ligands using HCHO.

diffraction showed that the Al_2O_3 support has a mixed structure of delta and gamma Al_2O_3 (see Fig. S4†). The XRD patterns of ALD TiO_2 overcoated Pd/Al_2O_3 catalysts (not shown) are identical to that of the bare Al_2O_3 substrate, suggesting that the ALD Pd and TiO_2 deposits are either amorphous, or too small for detection by conventional XRD.

Representative scanning transmission electron microscopy (STEM) images of the bare Al_2O_3 support and the as-prepared TiO_2 protected Pd_1 single atom catalysts are illustrated in Fig. 1. The ALD TiO_2 treatment markedly improved the dispersion of the Pd on the Al_2O_3 substrate. Compared with the clean Al_2O_3 surface shown in Fig. 1(a), white dots representing isolated Pd_1 atoms are clearly shown in STEM images in Fig. 1(b) after carrying out the synthesis strategy discussed in Scheme 1. Unfortunately, Pd nanoparticles (NPs) also co-exist with Pd_1 on the substrate (see Fig. S5†) with an average diameter of 3.4 ± 0.9 nm. Although the ratio of Pd_1 *vs.* Pd NPs is larger than 1000 : 1, only *ca.* 52% of the palladium was present as single atoms. TiO_2 cannot be clearly seen in the STEM images due to its small quantity and low contrast with the Al_2O_3 support. The surface composition of the Pd_1 catalysts was quantitatively analyzed using X-ray photoelectron spectroscopy (XPS). For the 1c, 7c and 14c TiO_2 thin film stabilized catalysts, the surface Ti/Al ratio increases with increasing TiO_2 ALD cycles from 0.65 to 1.04, while the Pd/(Ti + Al) ratio decreases from 0.16 to 0.05 (see Fig. 2). The Pd 3d XPS spectra for the as-prepared Pd catalysts show that the as-prepared Pd nanoparticles apparently have two peaks at 337.9 eV and 336.3 eV which are assigned to Pd^{2+} and Pd^0, respectively.[38,39]

In situ FTIR was performed in an ALD chamber under practical ALD conditions to understand the reason for the formation of Pd nanoparticles (see Fig. 3). The infrared peaks have been assigned in previous work.[29,38,40] The features at 1652 and 1605 cm^{-1} are assigned to the stretching vibration modes of C═O in the –hfac ligands. In particular, the peak at 1605 cm^{-1} is assigned to the C═O stretching vibration mode in the surface Pd(hfac) species, while 1652 cm^{-1} is related to the C═O stretching vibration mode in the surface –hfac species chemisorbed on the Al_2O_3 surface (*i.e.* Al(hfac)), where the hfac ligands have spilled over from the $Pd(hfac)_2$ during adsorption.[38] This feature at 1605 cm^{-1} almost completely disappeared after only 2 cycles of TiO_2 ALD, suggesting a reaction between the TiO_2 ALD precursors and the surface –Pd(hfac) species. As the –hfac ligands are thought to play an important role in stabilizing Pd_1 on the Al_2O_3 surface, the loss of –hfac may increase the Pd mobility leading to agglomeration, and Pd NP formation on the surface during TiO_2 ALD.

The thermal stability of the as-prepared Pd_1 catalysts under oxidation conditions was tested by calcination at 300 °C in air. Aberration corrected STEM images (see Fig. 4) revealed that the $14TiPd_1$ sample was relatively unchanged by calcination, and remains essentially as Pd_1 (Fig. 4e and f). In contrast, both 0TiPd and $7TiPd_1$ showed extensive aggregation to 4.6 ± 1.0 nm and 2.9 ± 0.7 nm, respectively, after 300 °C calcination. These results demonstrate that the nanocavity TiO_2 layer with an appropriate thickness can prevent the migration of Pd atoms and subsequent agglomeration at high temperature.

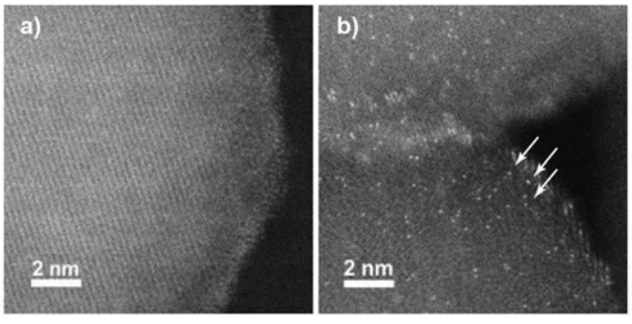

Fig. 1 HAADF-STEM images of (a) clean spherical aluminum oxide surface, and (b) thin film stabilized $7TiPd_1$ catalysts on aluminum oxide.

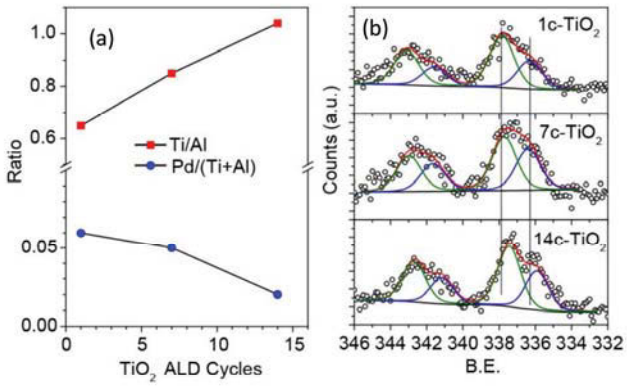

Fig. 2 (a) Ratio of surface species determined using XPS, (b) Pd 3d XPS spectra, black open circle, raw spectra; green and blue, peak contributions; red, sum of fitting; black, baseline.

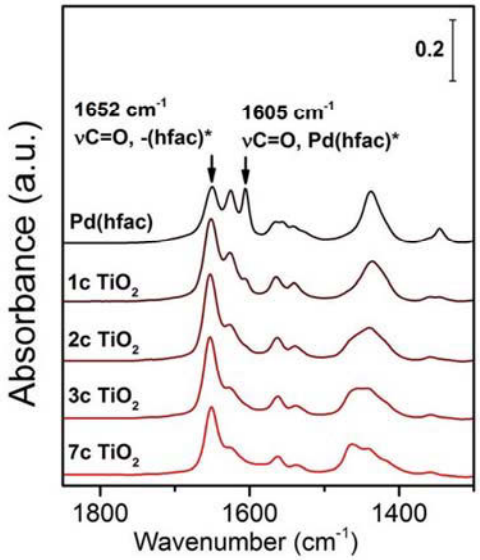

Fig. 3 Infrared absorbance spectra of $Pd(hfac)_2$ exposure and subsequent TiO_2 ALD cycle using $TiCl_4$ and H_2O as precursors.

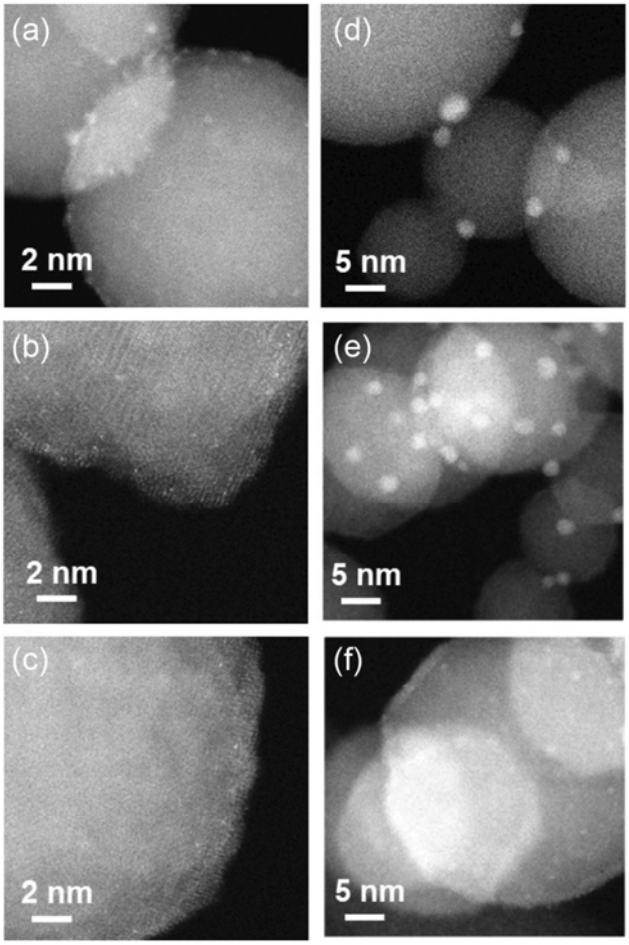

Fig. 4 Aberration corrected STEM images of (a) the as-prepared 0TiPd, (b) the as-prepared 7TiPd, (c) the as-prepared 14TiPd$_1$, (d) 0TiPd$_1$ after calcination, (e) 7TiPd$_1$ after calcination, (f) 14TiPd$_1$ after calcination. Calcination was performed at 300 °C in air.

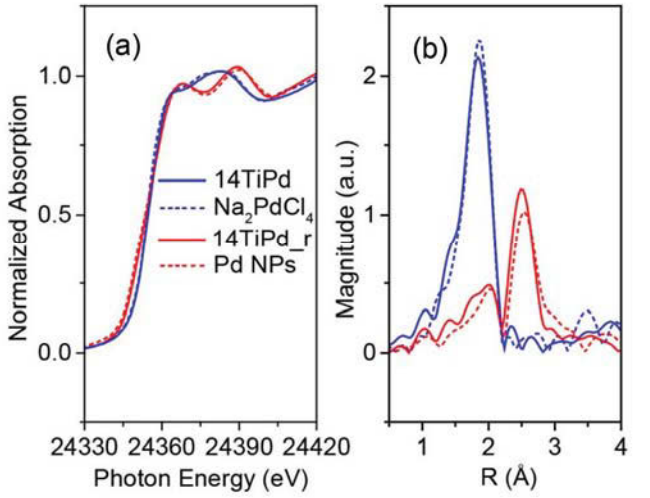

Fig. 5 Pd K-edge (a) XANES and (b) EXAFS Fourier transform of the Pd$_1$ catalysts and reference samples.

Table 1 Pd K edge EXAFS fits of the as-prepared Pd$_1$ catalysts before (1TiPd$_1$, 7TiPd$_1$ and 14TiPd$_1$) and after hydrogen reduction at 250 °C (1TiPd$_1$_r, 7TiPd$_1$_r and 14TiPd$_1$_r)

Sample	Scatter	CN	R, Å	DWF ($\times 10^3$)	E_0, eV
1TiPd$_1$	Pd–Cl	3.5	2.30	0.3	0.1
	Pd–O	0.5	2.02	0.7	4.6
1TiPd$_1$_r	Pd–Pd	3.6	2.77	2.0	−1.0
	Pd–Cl	0.6	2.29	0.3	−3.1
7TiPd$_1$	Pd–Cl	3.9	2.30	0.3	−0.2
	Pd–O	0.1	2.00	0.7	3.2
7TiPd$_1$_r	Pd–Pd	5.6	2.77	2.0	−0.7
	Pd–Cl	0.5	2.31	0.3	−1.4
14TiPd$_1$	Pd–Cl	3.9	2.30	0.3	−0.3
	Pd–O	0.1	1.99	0.7	2.4
14TiPd$_1$_r	Pd–Pd	5.6	2.77	2.0	−0.5
	Pd–Cl	0.6	2.31	0.3	−0.8

The thermal stability of the thin film stabilized Pd$_1$ catalysts under hydrogen reduction conditions was studied using X-ray absorption spectroscopy (XAS) at the Pd K edge. As shown in Fig. 5, both the X-ray absorption near edge structure (XANES) and the extended X-ray absorption fine structure (EXAFS) spectra of the as-prepared 14TiPd$_1$ catalyst resemble those of the Na_2PdCl_4 reference. After reduction in hydrogen at 250 °C, the XANES and EXAFS spectra of the reduced 14TiPd$_1$ catalyst (14TiPd$_1$_r) are similar to those of Pd NPs prepared using incipient wetness impregnation (IWI). The parameters extracted from fitting the extended X-ray absorption fine structure (EXAFS) spectra in K- and R-space are listed in Table 1 and the fitting quality is shown in Fig. S6 and S7,† respectively. The as-prepared Pd$_1$ atoms are coordinated with *ca.* 4 chlorine atoms. The presence of chlorine is due to the TiO_2 ALD process using $TiCl_4$ as a precursor. This residual Cl is consistent with $TiCl_4$ attacking the surface –Pd(hfac) species during TiO_2 ALD as postulated from the *in situ* FTIR measurements. The reduced Pd catalysts have coordination numbers from 3.6 to 5.6. As the coordination number of a Pd nanoparticle of 3–4 nm in diameter can be estimated to be about 9 to 10,[41] the ALD thin film stabilized Pd catalysts are likely to contain both single atoms and nanoparticles, consistent with the observation from the STEM imaging. Pd K edge XANES linear combination fittings (LCFs) were used to calculate the coordination of Pd. The results of XANES LCFs are similar to the results obtained from EXAFS fittings (see Fig. S8 and Table S2†).

In situ DRIFTS CO chemisorption has been an effective tool to assess the existence of site-isolated species such as Rh$_1$,[42] and Pt$_1$.[43] The CO molecules can only adsorb linearly on single atoms. The feature representing atop CO adsorbed on single atoms is normally distinguishable from that on nanoparticles. Although the infrared spectral assignment of CO adsorbed on Pd has been studied intensively,[44,45] the determination of the CO chemisorption feature on single site Pd$_1$ is not straightforward as CO can cause single atom sintering observed by Diebold and coworkers using scanning tunneling microscopy over Pd$_1$/Fe_3O_4 model catalysts.[46] Fig. 6 and S9† show CO adsorption on thin film stabilized Pd$_1$ at room temperature resulting in adsorption features as atop CO species

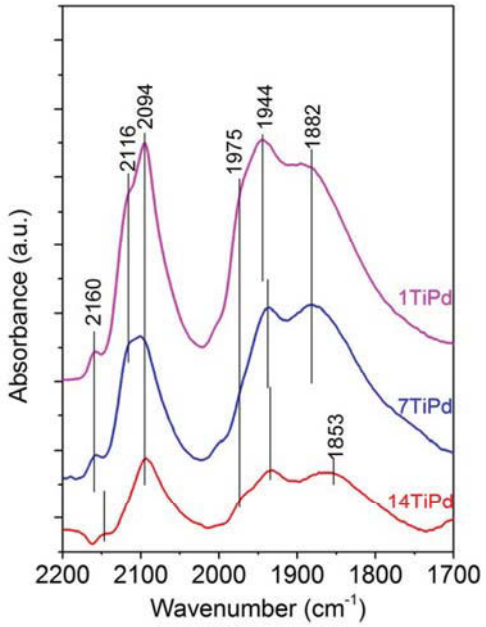

Fig. 6 DRIFTS spectra of CO adsorption. The spectra were obtained after room temperature purging of gas phase CO with He and reference to the background spectra recorded before exposure to CO.

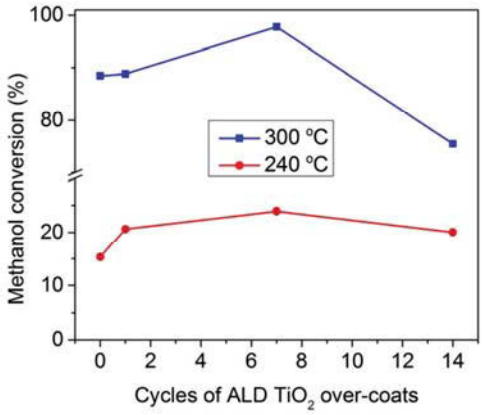

Fig. 7 Methanol conversion as a function of ALD TiO_2 cycles in the methanol decomposition reaction with error ± 10%.

($2160\ cm^{-1}$, $2116\ cm^{-1}$ and $2094\ cm^{-1}$), bridge-bonded CO ($1975\ cm^{-1}$ and $1944\ cm^{-1}$) and 3-fold hollow sites ($1882\ cm^{-1}$). The features at $2160\ cm^{-1}$, $2116\ cm^{-1}$ and $2094\ cm^{-1}$ can be assigned to CO chemisorption on Pd^{2+}, Pd^{+} and Pd^{0}, respectively.[47] The small feature at $2160\ cm^{-1}$ is most likely associated with the CO adsorption on single atom Pd_1, while the other two peaks represent CO adsorption on Pd nanoparticles.

With the small intensity of $2160\ cm^{-1}$ and the dominant features of CO chemisorption on bridge- and 3-fold hollow sites, we believe that agglomeration of adatom Pd occurs during the CO chemisorption, similar to what is observed in the Pd_1/Fe_3O_4 model catalyst system.[46] The intensities of these bands decreased and some of the bands shifted slightly with increasing TiO_2 ALD cycles, indicating that Pd is progressively covered by the ALD TiO_2. Similar results have been observed for Al_2O_3 ALD overcoats on the Pd surface and TiO_2 ALD on Au.[48,49]

The catalytic activity of the TiO_2 thin film stabilized Pd_1 catalysts was evaluated using methanol decomposition as a probe reaction. Fig. 7 shows the reactivity for methanol decomposition at 240 °C and 300 °C as a function of TiO_2 ALD cycles. The light-off curves during heating and cooling mostly overlapped with each other (see Fig. S10†), suggesting no significant changes such as sintering or coke deposition. The catalysts were also tested under methanol decomposition conditions at 300 °C for 24 hours without significant deactivation. The catalyst performance clearly depends on the cycles of the overcoat. At 240 °C, all three thin film stabilized Pd_1 catalysts showed enhanced performance than the Pd nanocatalysts. The 7c TiO_2 thin film stabilized Pd catalysts ($7TiPd_1$) showed the best performance with ~24% methanol conversion while Pd nanoparticles had close to ~15% methanol conversion. The enhanced performance can be explained by the enhanced thermal stability of the Pd_1 catalysts which possessed more surface active sites than the Pd nanoparticles, *i.e.*, all the Pd atoms in Pd_1 catalysts can potentially act as active sites while only the surface atoms on Pd nanoparticles can catalyze chemical reactions. The 14c TiO_2 thin film stabilized Pd_1 catalysts showed slightly lower conversion at ~20% than $7TiPd_1$ even though it had showed the best thermal stability observed by STEM. This seems to suggest that 14c TiO_2 not only deposits around Pd_1 to enhance its thermal stability but also starts to cover the Pd surface. This has been evidenced by the DRIFTS CO chemisorption studies where the intensity of the CO bands decreased with increasing TiO_2 ALD cycles. The blue shift, $29\ cm^{-1}$, observed on 3-fold hollow sites of CO on $14TiPd_1$ from the DRIFTS data suggests that at 14 cycles, the deposited TiO_2 mostly deposit on the Pd (111) sites on Pd nanoparticles.

At 300 °C, $7TiPd_1$ still showed the best performance with respect to methanol conversion. To our surprise, $14TiPd_1$ was the less active catalyst at 300 °C, even worse than the Pd nanoparticles. A simplified mechanism for the methanol decomposition reaction is summarized in the following two surface reactions (1) and (2).

$$CH_3OH_{(ad)} \rightarrow CO_{(ad)} + 4H_{(ad)} \quad (1)$$

$$2H_{(ad)} \rightarrow H_{2(g)} \quad (2)$$

Upon adsorption to the Pd surface, methanol can decompose into chemisorbed carbon monoxide $CO_{(ad)}$ and hydrogen $H_{(ad)}$ well below room temperature. Surface science studies performed by Goodman and Bowker showed that H_2 and CO desorbed from the Pd surface at 27 °C and 207 °C, respectively, indicating that methanol decomposition is desorption limited.[50] This is also known as the carbon monoxide self-poisoning effect: the CO product molecules strongly adsorb on the catalyst surface, preventing the methanol reactant from accessing the catalyst and the reaction terminates.

As CO is one of the products for methanol decomposition, a hypothesis is that CO binds much more strongly on Pd_1 than on Pd nanoparticles, which suppress the activity of Pd_1 catalysts. To test this hypothesis, EXAFS measurements at the Pd L_3 (3173 eV) edge were carried out to probe the adsorption of CO at room temperature and 250 °C. The palladium L_3 edge represents dipole-allowed 2p → 4d transition, and the L_3 absorption probes the density of states (DOS) of palladium d character. The L_3 edge is characterized by the presence of intense resonances, the "white line". Changes in the L_3 XANES white line after chemisorption of an adsorbate on the Pd surface reflect electronic structural changes caused by orbital hybridization. The ΔXANES (XANES spectrum of the precious metal with the adsorbate minus that of the clean surface) has a unique shape with respect to the type of adsorbate and the intensity increases with the adsorbate concentration, and therefore it can be used to both identify and quantify the adsorbates.[51,52] Fig. 8 shows Pd L_3 XANES and ΔXANES spectra for Pd NPs (0TiPd) and Pd_1 ($14TiPd_1$) catalysts in a steady state flow of helium and CO at 25 °C and 250 °C, respectively. For Pd NPs, there is a significant CO uptake at 25 °C because of the strong CO adsorption.

But at 250 °C, there is almost no CO coverage on the Pd surface, indicating a fast desorption of CO on the surface. In sharp contrast, even at 250 °C, there is still significant CO adsorbed on the Pd_1 atoms. Assuming that the CO adsorption sites at 25 °C are potential active sites for catalyzing methanol decomposition, and normalizing the CO coverage to these sites, *ca.* 70% of the surface adsorption sites were still covered by CO at 250 °C for $14TiPd_1$.

Therefore, the surface is still largely "poisoned" by the chemisorbed CO molecules. This result suggests that CO adsorbs much more strongly on supported Pd_1 single atoms than Pd nanoparticles. This is also consistent with the surface science studies on a series of size-selected Pd_n (n = 1–25) clusters, which reported that TiO_2 supported single atom Pd_1 showed the highest Pd 3d binding energy and lowest CO oxidation activity.[9] The authors ascribed this phenomenon to the stable valence structure of Pd_1/TiO_2.

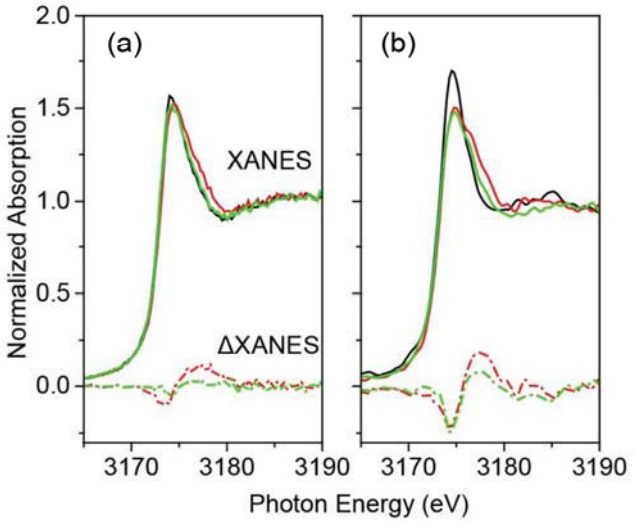

Fig. 8 Pd L_3 XANES spectra and ΔXANES spectra for (a) 0TiPd with adsorbed CO, (b) $14TiPd_1$. Black, He at 25 °C; red, CO at 25 °C; green, CO at 250 °C; dash dot line Pd L_3 ΔXANES with respect to Pd in He.

Conclusions

In summary, we developed a novel strategy to synthesize thermally stable single atom Pd_1 catalysts by combining Pd ALD and templated-TiO_2 ALD. Although there were Pd nanoparticles formed on the surface, *in situ* FT-IR under reaction conditions reveal that it can be avoided in the future by choosing mild precursors that would not attack the surface –Pdhfac species during the metal oxide ALD. Overall, the ALD TiO_2 overcoat dramatically enhanced the stability of single atom Pd_1 catalysts under both oxidation and reduction conditions. These thin film stabilized Pd_1 catalysts are promising catalysts for the methanol decomposition reaction. The reactivity seems strongly dependent on the cycles of overcoats, representing a combining effect of thermal stability and the amount of exposure sites of surface Pd. The single-atom Pd_1 catalysts protected by 14 cycle ALD TiO_2 showed greatly enhanced thermal stability with no obvious agglomeration after 300 °C calcination. Interestingly, it was also the least active catalysts for methanol decomposition at 300 °C. The $14TiPd_1$ catalysts have dramatically different chemical behavior as compared to Pd NPs as evidenced by the much stronger adsorption of CO on Pd_1 seen by *in situ* Pd L_3 edge XANES and ΔXANES.

Acknowledgements

We gratefully acknowledge support from the National Science Foundation (CBET-1511820) and Ralph E. Junior Faculty Enhancement Award from Oak Ridge Associated Universities. Part of the work including the methanol decomposition reaction and *in situ* DRIFTS study was conducted at the Center for Nanophase Materials Sciences, which is a DOE Office of Science User Facility. Use of the Advanced Photon Source was supported by the U. S. Department of Energy, Office of Science, Office of Basic Energy Sciences, under Contract No. DE-AC02-06CH11357. MRCAT operations are supported by the Department of Energy and the MRCAT member institutions.

References

1 M. Haruta, *Catal. Today*, 1997, **36**, 153–166.
2 A. M. Argo, J. F. Odzak and B. C. Gates, *J. Am. Chem. Soc.*, 2003, **125**, 7107–7115.
3 J. Guzman, S. Carrettin, J. C. Fierro-Gonzalez, Y. L. Hao, B. C. Gates and A. Corma, *Angew. Chem., Int. Ed.*, 2005, **44**, 4778–4781.
4 J. Hagen, *Industrial Catalysis*, Wiley-VCH, Mannheim, 2006.

5 C. H. Bartholomew and R. J. Farrauto, *Fundamentals of Industrial Catalytic Processes*, Wiley-AIChE, New York, 2nd edn, 2005.

6 C. K. Tsung, J. N. Kuhn, W. Y. Huang, C. Aliaga, L. I. Hung, G. A. Somorjai and P. D. Yang, *J. Am. Chem. Soc.*, 2009, **131**, 5816–5822.

7 U. Heiz, A. Sanchez, S. Abbet and W. D. Schneider, *J. Am. Chem. Soc.*, 1999, **121**, 3214–3217.

8 S. Abbet, A. Sanchez, U. Heiz, W. D. Schneider, A. M. Ferrari, G. Pacchioni and N. Rosch, *J. Am. Chem. Soc.*, 2000, **122**, 3453–3457.

9 W. E. Kaden, T. P. Wu, W. A. Kunkel and S. L. Anderson, *Science*, 2009, **326**, 826–829.

10 S. S. Lee, C. Y. Fan, T. P. Wu and S. L. Anderson, *J. Am. Chem. Soc.*, 2004, **126**, 5682–5683.

11 Y. Lei, F. Mehmood, S. Lee, J. Greeley, B. Lee, S. Seifert, R. E. Winans, J. W. Elam, R. J. Meyer, P. C. Redfern, D. Teschner, R. Schlogl, M. J. Pellin, L. A. Curtiss and S. Vajda, *Science*, 2010, **328**, 224–228.

12 M. A. Rottgen, S. Abbet, K. Judai, J. M. Antonietti, A. S. Worz, M. Arenz, C. R. Henry and U. Heiz, *J. Am. Chem. Soc.*, 2007, **129**, 9635–9639.

13 X. Tong, L. Benz, P. Kemper, H. Metiu, M. T. Bowers and S. K. Buratto, *J. Am. Chem. Soc.*, 2005, **127**, 13516–13518.

14 G. Kyriakou, M. B. Boucher, A. D. Jewell, E. A. Lewis, T. J. Lawton, A. E. Baber, H. L. Tierney, M. Flytzani-Stephanopoulos and E. C. H. Sykes, *Science*, 2012, **335**, 1209–1212.

15 B. T. Qiao, A. Q. Wang, X. F. Yang, L. F. Allard, Z. Jiang, Y. T. Cui, J. Y. Liu, J. Li and T. Zhang, *Nat. Chem.*, 2011, **3**, 634–641.

16 S. Sun, G. Zhang, N. Gauquelin, N. Chen, J. Zhou, S. Yang, W. Chen, X. Meng, D. Geng, M. N. Banis, R. Li, S. Ye, S. Knights, G. A. Botton, T.-K. Sham and X. Sun, *Sci. Rep.*, 2013, **3**, 1775.

17 H. Yan, H. Cheng, H. Yi, Y. Lin, T. Yao, C. Wang, J. Li, S. Wei and J. Lu, *J. Am. Chem. Soc.*, 2015, 137.

18 L. Wang, S. Zhang, Y. Zhu, A. Patlolla, J. Shan, H. Yoshida, S. Takeda, A. I. Frenkel and F. Tao, *ACS Catal.*, 2013, **3**, 1011–1019.

19 J. Lu, C. Aydin, N. D. Browning and B. C. Gates, *Angew. Chem., Int. Ed.*, 2012, **51**, 5842–5846.

20 M. Yang, L. F. Allard and M. Flytzani-Stephanopoulos, *J. Am. Chem. Soc.*, 2013, **135**, 3768–3771.

21 M. Yang, S. Li, Y. Wang, J. A. Herron, Y. Xu, L. F. Allard, S. Lee, J. Huang, M. Mavrikakis and M. Flytzani-Stephanopoulos, *Science*, 2014, **346**, 1498–1501.

22 E. Bayram, J. Lu, C. Aydin, A. Uzun, N. D. Browning, B. C. Gates and R. G. Finke, *ACS Catal.*, 2012, **2**, 1947–1957.

23 P. Bassler, H. G. Gobbel and M. Weidenbach, *Chem. Eng. Trans.*, 2010, **21**, 571–576.

24 T. A. Nijhuis, M. Makkee, J. A. Moulijn and B. M. Weckhuysen, *Ind. Eng. Chem. Res.*, 2006, **45**, 3447–3459.

25 T. Hayashi, K. Tanaka and M. Haruta, *J. Catal.*, 1998, **178**, 566–575.

26 J. Q. Lu, X. M. Zhang, J. J. Bravo-Suarez, K. K. Bando, T. Fujitani and S. T. Oyama, *J. Catal.*, 2007, **250**, 350–359.

27 N. Yap, R. P. Andres and W. N. Delgass, *J. Catal.*, 2004, **226**, 156–170.

28 X. F. Feng, A. Q. Wang, B. T. Qiao, J. Li, J. Y. Liu and T. Zhang, *Acc. Chem. Res.*, 2013, **46**, 1740–1748.

29 Y. Lei, J. L. Lu, H. Y. Zhao, B. Liu, K. B. Low, T. P. Wu, J. A. Libera, J. P. Greeley, P. J. Chupas, J. T. Miller and J. W. Elam, *J. Phys. Chem. C*, 2013, **117**, 11141–11148.

30 S. M. George, *Chem. Rev.*, 2010, **110**, 111–131.

31 F. Zaera, *J. Phys. Chem. Lett.*, 2012, **3**, 1301–1309.

32 J. Lu, J. W. Elam and P. C. Stair, *Surf. Sci. Rep.*, 2016, **71**, 410–472.

33 Z. Lu, O. Kizikaya, A. J. Kropf, M. Piernavieja-Hermida, J. T. Miller, R. Kurtz, J. W. Elam and Y. Lei, *Catal. Sci. Technol.*, 2016, DOI: 10.1039/C6CY00682E.

34 B. J. O'Neill, D. H. K. Jackson, J. Lee, C. Canlas, P. C. Stair, C. L. Marshall, J. W. Elam, T. F. Kuech, J. A. Dumesic and G. W. Huber, *ACS Catal.*, 2015, **5**, 1804–1825.

35 J. Lu, Y. Lei, K. C. Lau, X. Luo, P. Du, J. Wen, R. S. Assary, U. Das, D. J. Miller, J. W. Elam, H. M. Albishri, D. A. El-Hady, Y. K. Sun, L. A. Curtiss and K. Amine, *Nat. Commun.*, 2013, **4**, 2383.

36 J. Aarik, A. Aidla, H. Mandar and T. Uustare, *Appl. Surf. Sci.*, 2001, **172**, 148–158.

37 J. Aarik, A. Aidla, T. Uustare, M. Ritala and M. Leskela, *Appl. Surf. Sci.*, 2000, **161**, 385–395.

38 Y. Lei, B. Liu, J. Lu, J. A. Libera, J. P. Greeley and J. W. Elam, *J. Phys. Chem. C*, 2014, **118**, 22611–22619.

39 A. Gharachorlou, M. D. Detwiler, A. V. Nartova, Y. Lei, J. L. Lu, J. W. Elam, W. N. Delgass, F. H. Ribeiro and D. Y. Zemlyanov, *ACS Appl. Mater. Interfaces*, 2014, **6**, 14702–14711.

40 D. N. Goldstein and S. M. George, *Thin Solid Films*, 2011, **519**, 5339–5347.

41 A. I. Frenkel, C. W. Hills and R. G. Nuzzo, *J. Phys. Chem. B*, 2001, **105**, 12689–12703.

42 J. C. Matsubu, V. N. Yang and P. Christopher, *J. Am. Chem. Soc.*, 2015, **137**, 3076–3084.

43 K. Ding, A. Gulec, A. M. Johnson, N. M. Schweitzer, G. D. Stucky, L. D. Marks and P. C. Stair, *Science*, 2015, **350**, 189–192.

44 K. Kovnir, M. Armbruster, D. Teschner, T. V. Venkov, L. Szentmiklosi, F. C. Jentoft, A. Knop-Gericke, Y. Grin and R. Schlogl, *Surf. Sci.*, 2009, **603**, 1784–1792.

45 H. L. Abbott, A. Aumer, Y. Lei, C. Asokan, R. J. Meyer, M. Sterrer, S. Shaikhutdinov and H. J. Freund, *J. Phys. Chem. C*, 2010, **114**, 17099–17104.

46 G. S. Parkinson, Z. Novotny, G. Argentero, M. Schmid, J. Pavelec, R. Kosak, P. Blaha and U. Diebold, *Nat. Mater.*, 2013, **12**, 724–728.

47 D. Tessier, A. Rakai and F. Bozon-Verduraz, *J. Chem. Soc., Faraday Trans.*, 1992, **88**, 741–749.

48 H. Feng, J. Lu, P. C. Stair and J. W. Elam, *Catal. Lett.*, 2011, **141**, 512–517.
49 C. Wang, H. Wang, Q. Yao, H. Yan, J. Li and J. Lu, *J. Phys. Chem. C*, 2015, **120**, 478–486.
50 S. M. Francis, J. Corneille, D. W. Goodman and M. Bowker, *Surf. Sci.*, 1996, **364**, 30–38.
51 Y. Lei, H. Y. Zhao, R. Diaz-Rivas, S. Lee, B. Liu, J. L. Lu, E. A. Stach, R. E. Winans, K. W. Chapman, J. P. Greeley, J. T. Miller, P. J. Chupas and J. W. Elam, *J. Am. Chem. Soc.*, 2014, **136**, 9320–9326.
52 Y. Lei, J. Jelic, L. C. Nitsche, R. Meyer and J. T. Miller, *Top. Catal.*, 2011, **54**, 334–348.